

# Modelling Kinematics and Dark Matter: The Halos of Elliptical Galaxies\*

Ortwin Gerhard

Astronomisches Institut, Universität Basel, Venusstrasse 7, CH-4102 Switzerland

**Abstract.** This review is focussed on the outer halos of elliptical galaxies. Its emphasis is on (i) planetary nebulae as test particles to trace the stellar kinematics at large radii, (ii) the observed angular momentum in elliptical galaxy halos and its theoretical relevance, (iii) dynamical modelling of stellar-kinematic data, and (iv) a discussion of the evidence for dark matter halos in ellipticals from a wide range of measurements.

## 1 Introduction

In current hierarchical theories, elliptical galaxies represent an advanced stage of the galaxy formation process: they are massive galaxies found in dense environments. They reflect ‘early’ conditions in galaxy formation as well as subsequent merging processes, making the study of their properties particularly interesting.

However, their old stellar populations and complicated orbital structure make many important questions harder to answer for ellipticals than for spirals. This includes cosmological questions about their ages and precise formation mechanism, about the concentration of their dark matter halos, and the segregation of baryonic matter, as well as dynamical questions about the orbit distribution and total angular momentum, to name only a few.

The subject of this review is the halos of elliptical galaxies and how planetary nebulae observations and dynamical modelling can help answer some of these questions. Several other papers in this session elaborate on the topics discussed here.

## 2 Planetary Nebulae as Kinematic Tracers

Planetary Nebulae (PNe) are excellent test particles to trace the kinematics in the outer halos of elliptical galaxies. They occur as a brief stage in the late evolution of stars with masses between  $\sim 0.8\text{--}8 M_{\odot}$ , when these stars evolve from the asymptotic giant phase to their final white dwarf stage. Their nebular gas envelope converts up to 15% of the central star’s radiation energy to photons in the characteristic  $\lambda 5007$  [OIII] emission line [1]. From this emission line, PNe can be identified and their radial velocities measured spectroscopically at distances of up to 20–30 Mpc. With 8m class telescopes [2] or the special-purpose Planetary

\* To appear in: Planetary Nebulae beyond the Milky Way, ESO Astrophysics Symposia, eds. Stanghellini, L., Walsh, J. R., Douglas, N. G., Springer, Heidelberg.

Nebula Spectrograph (PN.S) [3], several hundred PNe have been found in giant elliptical galaxies with distance up to the Virgo cluster. The PN number density approximately follows the surface density of stars; thus a few tens of PNe can be used to measure the stellar kinematics at several effective radii  $R_e$ , where the surface brightness is too faint for absorption line spectroscopy (ALS).

From these PN velocities, constraints on the angular momentum, dynamics, and mass distribution in the outer halos of ellipticals can be derived; these are important to compare with predictions from theories of galaxy formation.

In this analysis, it is always advantageous if additional information can be included. Especially, stellar kinematics from ALS are highly desirable (i) to determine the mass-to-light ratio in the inner, presumably baryon-dominated parts of the galaxy, and (ii) to narrow down the range of permitted dynamical anisotropies at 1-2 effective radii [4]. Also, globular cluster (GC) velocities are now becoming available in substantial numbers around luminous ellipticals. While the spatial distribution and dynamics of the globular cluster system may be different from those of the stars, analysis of these velocities gives additional constraints on the common gravitational potential [5]. Lastly, an ideal case is when the galaxy potential is narrowly constrained from Chandra or XMM X-ray observations [6]. Then the information obtained with the PN kinematics can be used entirely for inferring the orbital structure of the outer stellar halo in the known potential. These issues are further discussed later; the present section is concerned with PNe as kinematic tracers.

## 2.1 Does the PN Number Density Follow Light?

Although PNe are representative for the bulk of all stars, there are some population effects that can bias their number density profile with respect to the galaxy's luminosity profile. The PN luminosity function (PNLF) is observed to have a near-universal form and bright cut-off magnitude [7]. Then the quantity  $\alpha_{X,n}$  is defined as the ratio of the number of PN in a stellar population,  $n$  magnitudes down the PNLF from the cut-off magnitude, to its total stellar luminosity, in a specified wavelength band  $X$ . While the bolometric  $\alpha_{\text{bol},\infty}$  is expected to be nearly independent of stellar population [8], Hui *et al.* show that the blue  $\alpha_{B,2.5}$  depends on colour B-V, decreasing by a factor of 4 from the M31 bulge to the reddest elliptical galaxies [9]. Age, or metallicity, or both, must influence  $\alpha_{B,2.5}$ . Theoretical models predict that the brightest PNe in B have central stars with progenitor masses  $\sim 2.5 M_\odot$  [10], with luminosity also dependent on uncertain post-AGB evolution parameters and metallicity. The presence of a younger population in elliptical galaxies, whether made in situ or accreted, could thus change the number of bright PNe significantly. Real ellipticals can have colour and metallicity gradients. Therefore it is prudent to check carefully whether the observed (usually magnitude-limited) PNe samples do indeed trace light.

Observational tests of this question have been carried out in a number of galaxies, including M31, Cen A, the Leo group galaxies NGC 3377, 3379 and 3384, several Virgo ellipticals, the Fornax galaxies NGC 1399 and NGC 1404, and NGC 4697 [2,7,9,11]. Generally, the number of PNe as a function of isophote

follows the luminosity distribution for radii outside  $\sim 1 - 2'$ , in some cases very well. At smaller radii some PNe are lost against the bright background of the galaxy, and the PNe no longer track the luminosity profile. A colour gradient such that the inner parts of the galaxy are redder with fewer PN per blue light may further decrease the number of PNe per unit light there; NGC 4697, for example, has a slight gradient of this kind [12].

## 2.2 Do the PN Kinematics Follow the Absorption Line Stellar Kinematics?

If the distribution of PNe follows light, the PNe can be considered as faithful tracers also for the stellar kinematics. A test of this is to compare the rotation velocities  $v$  and velocity dispersions  $\sigma$  obtained from PN radial velocities with those from ALS, taking into account the greater smoothing of the PN velocity field due to spatial averaging. Mendez used his sample of 535 PN velocities in NGC 4697 for a simple comparison [2]. His sample, restricted to a stripe around the major axis, indeed followed the rotation seen in the ALS data; however, the number of PNe per mean velocity point is  $\sim 10$  and so the errors are large,  $\sim 50 \text{ km s}^{-1}$ . Similarly, the PN velocity dispersions in major axis sectors were consistent with the ALS dispersions within  $\sim 20 \text{ km s}^{-1}$ .

In such a case the PN velocities and the ALS velocity measurements can be simply combined in modelling the stellar kinematics. Even the incompleteness in the center does not present a problem, because the probability of losing a PN against the bright galaxy background is uncorrelated with its radial velocity. Then only the PN velocities, but not their radial distribution must be used in the modelling. If, on the other hand, because of an outward colour gradient and the observed dependence of  $\alpha_B$  on colour, the distribution of PNe is more extended than the stellar light, say, then the PNe velocity dispersions would overestimate the stellar velocity dispersions, as can be seen most easily from the spherical Jeans equation. In this case, the PNe would have to be included in the modelling as a separate test particle distribution.

Another kinematic bias can occur for elliptical galaxies in galaxy clusters, in that the PN samples, particularly in the outer galactic halo, can be contaminated by intracluster PNe [13]. ICPNe would be difficult to disentangle from galactic PNe when the velocity dispersions of the galaxy and its host cluster are comparable, such as for NGC 1399 in the Fornax cluster.

## 2.3 How Many PNe Velocities Are Needed for Orbital and Potential Analysis?

With a few tens of PN velocities it is possible to detect a clear trend of rotation in the outer halo; see, e.g., the work of Arnaboldi *et al.* for NGC 4406 and NGC 1316 [13, 14]. To determine the detailed shape of the rotation velocity field requires substantially larger samples. Fig. 1, due to N. Sambhus, shows the results of fitting the velocities of approximately 200 PNe from PN.S observations [15] in the E0/1 galaxy NGC 3379 with a non-parametric spline method. The

velocity field shows a peak-to-peak rotation of  $\sim 100 \text{ km s}^{-1}$  at  $\sim 100''$ , with a subsequent decline out to  $\sim 300''$ , confirmed by the rotation along the line of maximum gradient. However, both the detailed shape of the rotation curve and the reality of the apparent asymmetry in the velocity field remain uncertain. For comparison, SAURON data show a clear rotation gradient in the central  $20''$ , which is unresolved in the PN velocities [16]. The conclusion from this is that PN velocities should be used as an outward extension of the ALS velocity measurements whenever possible [14].

The second important application of PN velocities is to help determine the masses of ellipticals in their outer regions, where the dark matter halos should begin to dominate. Because of the large freedom in the orbital structure and velocity anisotropy in elliptical galaxies, this is not an easy task. If no other kinematic constraints are available, Merritt has estimated that at least many hundreds of PN velocities would be required [17]. Thus, it is again advantageous to use the PN data in conjunction with ALS velocities and other data. From ALS data out to  $\sim 2R_e$ , including line profile shape parameters  $h_3$  and  $h_4$ , a range of dynamical models and gravitational potentials can be determined that are consistent with these data. Within these models, the implied orbital anisotropy and halo mass are correlated. Then only a few tens of PN velocities beyond  $2R_e$  are needed to further narrow down the permitted dynamics and mass distribution [4].

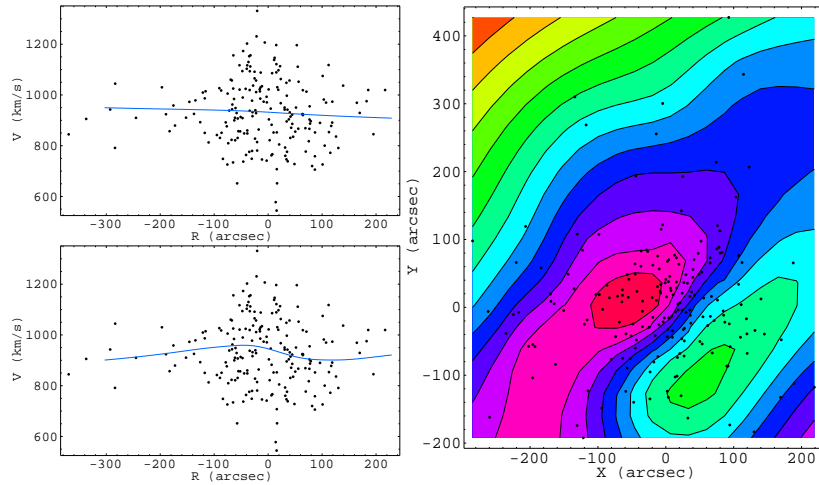


**Fig. 1.** Velocity field and streaming velocities from  $\sim 200$  PNe in NGC 3379. The right-hand figure shows a smoothed spline model for the projected mean velocity, derived from the PN velocities; contour spacing is  $10 \text{ km s}^{-1}$  and the galaxy center is at  $(0,0)$ . The two plots on the left show fits with different smoothing to the distribution of PN velocities versus distance along the direction of maximum gradient.

### 3 Angular Momentum in the Outer Parts of Ellipticals

One of the most interesting early results obtained with PNe was the discovery of rapid rotation in the halos of the giant elliptical galaxies Centaurus A, NGC 1399, and NGC 1316 [18, 14]. The PNe radial velocity fields in these early-type galaxies show that their outer halos are rapidly rotating, and that these galaxies contain comparable angular momentum to spiral galaxies of similar luminosity. Recent work on several further ellipticals has shown that most of these do not rotate rapidly at large radii; see diagram in [19]. There appears to be a range of outer rotation properties observed.

The amount of rotation in the halos of elliptical galaxies is a valuable probe for how these systems formed. Elliptical galaxies are now believed in general terms to form by merging processes; what is less clear is the kind of progenitors that dominated in the formation of the present population of ellipticals. Spiral-spiral galaxy mergers, observed in the local universe and spurring Toomre's original merger hypothesis [20], give remnants that morphologically and kinematically resemble elliptical galaxies in many ways [21]. Equal-mass mergers have low  $v/\sigma \sim 0 - 0.2$  within  $R \lesssim R_e$ , as observed for giant ellipticals, due to angular momentum transfer from inner regions to the extended outer halos by dynamical friction in the merger. These remnants can, however, contain significant angular momentum at large radii, reaching  $v/\sigma \sim 0.2 - 0.5$ , even though a lot of spin angular momentum is carried away by material in the tidal tails. Unequal-mass mergers rotate faster than equal-mass mergers. As argued in [21], binary mergers of disk galaxies may be the main formation mechanism of low- and intermediate mass ellipticals.

An alternative merging channel to form an elliptical is through multiple major and minor mergers in a compact group of galaxies [22]. In this case the tidal forces are more effective in disrupting the progenitors before coalescence, so dynamical friction is less effective. As a result, the remnants have more angular momentum in their inner parts than spiral-spiral mergers, placing them not far from the oblate-isotropic line in the  $v/\sigma - \epsilon$  diagram, and their outer parts may reach  $v/\sigma \sim 1$ .

Computations of the angular momentum of dark matter halos growing by merging and accretion in hierarchical universes result in low spin parameter  $\lambda$  and low  $v/\sigma$  [23]. Interestingly, the values of these parameters in the evolution of individual halos are most likely to increase in major mergers, and generally decrease in multiple accretion of satellites. If this is indicative for the luminous components also, then ellipticals that were last shaped by a major merger should contain the highest angular momenta. The rotation velocities in the remnant halos are fairly constant with radius, however, confirming that the dissipation and dynamical friction processes acting specifically on the baryonic component are crucial for shaping the angular momentum distributions in elliptical galaxies.

These results show that there is no simple, one-to-one correspondence between angular momentum at large radii and formation mechanism. For example, of the ellipticals with outer PN kinematics, Centaurus A is believed to have formed from the merger of two disk galaxies; in this galaxy  $v/\sigma$  rises to  $\sim 1$

beyond  $R = 15$  kpc [18]. However, how much angular momentum resides in the outer halos of elliptical galaxies is clearly a key issue which, when understood for a representative sample of elliptical galaxies, will be crucial for determining the merging channel that dominated their formation. This is a research program that can ideally be tackled by PNe radial velocity measurements with the PN.S.

## 4 Dynamical Analysis of Kinematic Data

This Section gives a brief overview of how the gravitational potential of an elliptical galaxy can be inferred from stellar-kinematic data. These data may include PN velocities, which individually sample the stellar line-of-sight velocity distributions  $L(v)$  (hereafter LOSVD) at their positions in the galaxy image, as well as ALS spectroscopy measurements of the first few moments of the LOSVD, at a set of 1D or 2D binned positions.

As is well known, velocity dispersion profile measurements (and streaming velocities, if the galaxy rotates) do not suffice to determine the distribution of mass with radius, due to the degeneracy with orbital anisotropy. With very extended measurements a constant  $M/L$  model can be ruled out (e.g., [18]), but the detailed  $M(r)$  still remains undetermined. Thus mass determination in elliptical galaxies always involves determining the orbital structure at the same time, and requires a lot of data. LOSVDs from absorption line profile shapes provide additional data with which the degeneracy between orbit structure and mass can largely be broken. Simple spherical models are useful to illustrate this [24]: at large radii, radial orbits are seen side-on, resulting in a peaked LOSVD (positive Gauss-Hermite parameter  $h_4$ ), while tangential orbits lead to a flat-topped or double-humped LOSVD ( $h_4 < 0$ ). Similar considerations can be made for edge-on or face-on disks [25] and spheroidal systems [26].

One may think of the LOSVDs constraining the anisotropy, after which the Jeans equations can be used to determine the mass distribution. However, the gravitational potential influences not only the widths, but also the shapes of the LOSVDs (see illustrations in [24]). Furthermore, eccentric orbits visit a range of galactic radii and may therefore broaden a LOSVD near their pericentres as well as leading to outer peaked profiles. Thus, in practice, the dynamical modelling to determine the orbital anisotropy and gravitational potential must be done globally, and is typically done in the following steps:

- (0) choose geometry (spherical, axisymmetric, triaxial);
- (1) choose dark halo model parameters, and set total luminous plus dark matter potential  $\Phi$ ;
- (2) write down a composite distribution function (DF)  $f = \sum_k a_k f_k$ , where the  $f_k$  can be orbits, or DF components such as  $f_k(E, L^2)$ , with free  $a_k$ ;
- (3) project the  $f_k$  to observed space,  $p_{jk} = \int K_j f_k d\tau$ , where  $K_j$  is the projection operator for observable  $P_j$ , and  $\tau$  denotes the line-of-sight coordinate and the velocities;
- (4) fit the data  $P_j = \sum_k a_k p_{jk}$  for all observables  $P_j$  simultaneously, minimizing a  $\chi^2$  or negative likelihood, and including regularization to avoid spurious

large fluctuations in the solution. This determines the  $a_k$ , i.e, the best DF  $f$ , given  $\Phi$ , which must be  $f > 0$  everywhere;

(5) vary  $\Phi$ , go back to (1), and determine confidence limits on the parameters of  $\Phi$ .

If the mass distribution and gravitational potential are known from analysis of, e.g., X-ray data, step (5) can be omitted. Because this eliminates the degeneracy with orbital anisotropy, considerably fewer data are then needed.

Such a scheme has been employed regularly to model spherical and axisymmetric galaxies [e.g., 4,27], using mostly orbits (“Schwarzschild’s method”) and, more rarely, distribution function components. Discrete velocity data were modelled in [e.g., 5,17]. The modelling techniques used to constrain black hole masses from nuclear kinematics and dark halo parameters from extended kinematics are very similar.

Line-profile shape parameter measurements are now available for many nearby ellipticals, but those reaching to  $\sim 2R_e$  are still scarce [e.g., 28, 4]. Modelling of the outer mass profiles of ellipticals from such data has been done for some two dozen round galaxies in the spherical approximation, and for a few cases using axisymmetric three-integral models.

From recent SAURON integral field measurements it has become clear that the kinematics of many elliptical galaxies show features incompatible with axisymmetry [16]. This has motivated Verolme *et al.* to extend Schwarzschild’s method to triaxial models [29], a development that has only recently become possible with the increase of available computing power. In parallel, adaptive N-body codes are being developed that use the algorithm of Syer & Tremaine for training N-body systems to adapt to a specified set of data constraints [30]. These latter models have the additional advantage of simultaneously providing a check for the model’s dynamical stability. One application has been to the rotating Galactic bar; work currently in progress is on axisymmetric and rotating triaxial galaxies.

## 5 The Dynamics and Dark Matter Halos of Elliptical Galaxies

### 5.1 Results from Dynamical Analysis of Absorption Line Profiles

Giant ellipticals with  $L \gtrsim L_*$  are typically fit best by dynamical models that have near-isotropic to modestly radially anisotropic velocity dispersions at intermediate radii,  $0.5 - 1R_e$  [4,27,31]. This is based on spherical and axisymmetric three-integral models of about two dozen ellipticals. In ellipticals less luminous than  $M_B = -19.5$  rotation is important and, moreover, these galaxies become rotation-dominated ( $v/\sigma \sim 2$ ) at  $1 - 2R_e$ , similar to disk-dominated S0 galaxies [32].

Most of the results on dark matter halos in ellipticals obtained from ALS data to  $2R_e$  are based on spherical models for round ellipticals. [4,31] analyzed the line-profile shapes of a sample of 21 mostly luminous, slowly rotating, and

nearly round elliptical galaxies in a uniform way, using spherical DF models. Intrinsic deviations from sphericity and embedded, near-face-on disks can play a role in only a small number of these bright galaxies. Nevertheless, a similar study using three-integral axisymmetric models of near-edge-on galaxies avoiding these issues will be very worthwhile. For these reasons the three-integral models of Matthias & Gerhard for the boxy E4 elliptical galaxy NGC 1600 provide some of the strongest evidence for radial anisotropy, because this galaxy must be viewed nearly edge-on [27].

The sample of Kronawitter *et al.* [4] includes a subsample with mostly new extended kinematic data, reaching to  $\sim 2R_e$ , and a subsample based on the less extended older data of [28]. Based on these data and on photometry, non-parametric spherical models were constructed from which circular velocity curves, anisotropy profiles, and radial profiles of  $M/L$  were derived, including confidence ranges. The circular velocity curve (CVC) for test particles on circular orbits of varying radius is a convenient measure of the potential, even though luminous elliptical galaxies do not rotate rapidly. The CVCs of the elliptical galaxies analysed by [4,31] are flat to within  $\simeq 10\%$  for  $R \gtrsim 0.2R_e$  to  $R \gtrsim 2R_e$ , independent of luminosity (Fig. 2). This argues against strong luminosity segregation in the dark halo potential.

The dynamical models imply small to modest amounts of dark matter within  $2R_e$  [4,31]. However, constant  $M/L$  models can be ruled out only for 7/21 ellipticals in this sample, at the  $2\sigma$  level. There are ellipticals in this sample which are very well represented by constant  $M/L$  models, and no indication for dark matter within  $2R_e$ , and others where the best dynamical models result in local  $M/L_{BS}$  of 15-30 at  $2R_e$ . Likewise, Magorrian & Ballantyne [25] find evidence for additional dark matter only in a subset of their galaxies, using constant-anisotropy spherical modelling. I.e., despite the uniformly flat CVCs, there is a spread in the ratio of the CVCs from luminous and dark matter. As in spiral galaxies, the combined rotation curve of the luminous and dark matter is flatter than those for the individual components (“conspiracy”).

In the models with maximum stellar mass, the dark matter contributes  $\sim 10 - 40\%$  of the mass within  $R_e$ . The flat CVC models, when extrapolated beyond the range of kinematic data, predict equal interior mass of dark and luminous matter at  $\sim 2 - 4R_e$ , consistent with results from X-ray analyses. Even in maximum stellar mass models, the implied halo core densities and phase-space densities are at least  $\sim 25$  times larger and the halo core radii  $\sim 4$  times smaller than in maximum disk spiral galaxies with the same circular velocity [33]. This could imply that some elliptical galaxy halos collapsed at high redshifts or perhaps even that some of their dark matter might be baryonic.

**Dust and Scattered Light?** Baes & Dejonghe have argued that scattered light from a high-velocity nucleus might give rise to broad wings in the LOSVD at large radii, in such a way as to mimic a dark matter halo in dynamical analysis [34]. This requires an optical depth  $\tau \simeq 1$ , i.e., that elliptical galaxies are on the verge of opaqueness. No such effect on the surface density of background



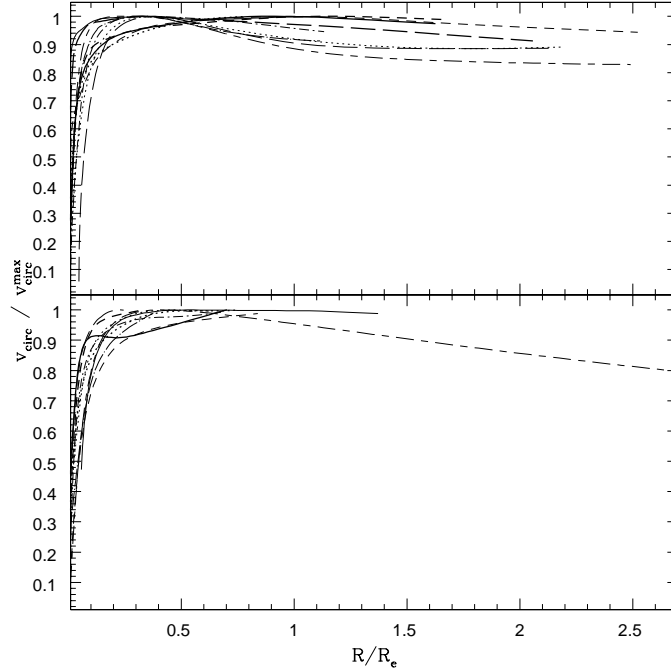


**Fig. 2.** “Best model” circular velocity curves of all galaxies from the sample of [4], plotted as a function of radius scaled by the effective radius  $R_e$ , and normalized by the maximum circular velocity. The upper panel shows the galaxies from the extended kinematics subsample, the lower panel the galaxies from the subsample with older data from [28]. (Figure from [31].)

galaxies is known to this author. A direct test is moreover possible when velocity measurements are available simultaneously from ALS data and from PNe, as the PN velocities are unaffected (e.g., NGC 4697 above), or when mass determinations are possible with independent techniques (e.g., NGC 1399 below). Also, the effect should be absent when the dispersion profile is constant; one such case in the sample of [4] is NGC 7626.

## 5.2 Results from Analyses Including PN or GC Velocities

Because the dark matter fraction inside  $2R_e$  is still modest, and the orbit structure in the outer main bodies of ellipticals is not well-constrained by data that end at  $2R_e$ , it is important to include discrete velocity data from planetary nebulae (PN) or globular clusters (GC) that reach to larger radii.

The results so far are mixed. PNe velocity dispersions in several intermediate luminosity ellipticals were found to decline with radius, and to require little if

any dark matter at  $2 - 5R_e$  [2,15]. Two of these (NGC 3379, 4494) were also part of the sample of [4,31], but were consistent with constant M/L also in that study. NGC 3379 has been argued to be a face-on S0 and a weakly triaxial system viewed face-on [35]. This would seem to be not a likely explanation for several galaxies at the same time, unless selecting round galaxies introduces a significant bias in this sense. It is comforting that the near-edge-on, similar luminosity NGC 4697 also has little evidence for dark matter [2]. See Romanowsky's paper for further discussion [19]. In Cen A, the observed PN kinematics do require a dark halo, consistent with the GC velocities, but the implied  $M/L_B$  is noticeably low [18, 36] when compared with values determined from the hot gas in X-ray bright ellipticals. A similar, mild gradient in  $M/L_B$  was inferred from PN velocities in NGC 1316 [14]. In several further elliptical galaxies, globular cluster velocities were used to estimate host galaxy masses, increasing outwards to several effective radii, but no  $M/L_B$  values were given [37].

Two interesting cases are the central galaxies of the Fornax and Virgo clusters, NGC 1399 and M87. In NGC 1399, the dynamical models for the ALS kinematics, predicting significantly increased  $M/L_B$  already at  $1 - 2R_e$  [4], the PN and GC velocities [5,18,38], and the ROSAT and ASCA X-ray data [39] imply a steady outward rise in  $M/L_B$ . The PN and GC velocities are in the right radial range to allow a study of the transition between the potential of the central NGC 1399 galaxy and the potential of the Fornax cluster. Similarly, from a study of the stellar kinematics and the GC velocities around M87, and a comparison to the X-ray mass profile, Romanowsky & Kochanek [5, see also 40] find a rising circular velocity curve, and suggest that the potential of the Virgo cluster may already dominate at  $r \sim 20$  kpc from the center of M87. The dark matter distribution inferred by them is in agreement with that inferred from the X-ray data [6].

### 5.3 Results from Gas Rotation Measurements

Generally, elliptical galaxies do not contain cold gas disks or rings that can be used to measure their halo circular velocities, but there are some notable exceptions. One such example is the early-type galaxy IC 2006 in the Fornax cluster. This galaxy has a remarkably axisymmetric HI ring extending from  $0.5 - 6R_e$ , with circular velocity nearly constant in this range of radii. In this galaxy,  $M/L$  rises strongly with radius, signifying a nearly axisymmetric dark halo [41].

Other ellipticals with settled HI disks are described in [42]. These galaxies probably acquired the HI gas by accretion. The dynamical interpretation requires understanding the shape of the potential. In several of these ellipticals,  $M/L_B$  shows a substantial increase with radius, e.g., NGC 2974, NGC 3108, NGC 4278. In NGC 3108, again the rotation curve is flat, to  $6R_e$ , in agreement with the results from analysing stellar kinematics discussed above.

#### 5.4 Results from Modelling X-ray Data

The hot X-ray emitting gas in luminous ellipticals is another means to estimate the gravitational potential. This requires measuring the X-ray emissivity and temperature. Typical temperature profiles are nearly constant. Some problems are that point sources must be removed from the emission maps, requiring high spatial resolution, and that the assumed hydrostatic equilibrium may not be strictly fulfilled. However, any gas motions will have velocities of order the sound speed, so the error made with this assumption is not likely to be very large.

X-ray mass measurements have been made regularly as new X-ray missions were flown, but have tended to concentrate on a small number of galaxies. With the new high-spatial and spectral resolution and high-sensitivity data from Chandra and XMM this situation may soon change. In the detailed analyses so far,  $M/L$  ratios of  $\sim 50$  at 10's of kpc have been found in, e.g., NGC 1399, M87, NGC 4472, NGC 4636, NGC 507, NGC 720 [6,39,43]; these galaxies are often the centers of galaxy clusters, however. Ubiquitous halos have furthermore been found in studies of the family properties of ellipticals from X-ray data [44].

#### 5.5 Conclusion

In addition to the body of evidence reviewed here, studies of satellite dynamics from SDSS data indicate large  $M/L \sim 100 - 200$  at radii  $260h^{-1}$  kpc in  $0.5 - 3L_*$  galaxies, and gravitational lensing studies indicate nearly isothermal mass profiles (constant CVCs) with a modest dark matter fraction inside  $2R_e$  [e.g., 45]. Space did not permit a detailed discussion of these issues here.

Alltogether the case is strong that, like all galaxies, elliptical galaxies have dark matter halos surrounding them, with most inner circular velocity curves nearly flat. But there may be some intermediate luminosity objects in which the halos are more diffuse. Future work to understand this is clearly worthwhile.

#### References

1. M. Dopita, G.H. Jacoby, E. Vassiliadis: ApJ, **389**, 27 (1992)
2. R. Mendez *et al.*: ApJ, **563**, 135 (2001)
3. N. Douglas *et al.*: PASP, **114**, 1234 (2002) and this proceedings
4. R.P. Saglia *et al.*: AJ, **119**, 153 (2000); A. Kronawitter *et al.*: A&AS, **144**, 53 (2000)
5. M. Kissler-Patig *et al.*: AJ, **115**, 105 (1998); A.J. Romanowsky, C.S. Kochanek: ApJ, 553, 722 (2001)
6. D.A. Buote *et al.*: ApJ, **577**, 183 (2002); K. Matsushita *et al.*: A&A, **386**, 77 (2002)
7. G. Jacoby: ApJ, **339**, 39 (1989); R. Ciardullo *et al.*: ApJ, **339**, 53 (1989); R. Ciardullo: in *Stellar Candles for the Extragalactic Distance Scale*, ed. by D. Alloin, W. Gieren, Lect. Notes Phys., **635**, 243 (2003)
8. A. Renzini, A. Buzzoni: in *Spectral Evolution of Galaxies*, ed. by C. Chiosi, A. Renzini (Reidel, Dordrecht 1986), p. 195; A. Buzzoni, M. Arnaboldi: this proceedings
9. X. Hui *et al.*: ApJ, **414**, 463 (1993)
10. P. Marigo *et al.*: A&A, **423**, 995 (2004)

11. R. Ciardullo, G.H. Jacoby, H.C. Ford: ApJ, **344**, 715 (1989); G.H. Jacoby, R. Ciardullo, H.C. Ford: ApJ, **356**, 332 (1990); McMillan, R. Ciardullo, G.H. Jacoby: ApJ, **416**, 62 (1993)
12. P. Goudfrooij: A&AS, **104**, 179 (1994)
13. M. Arnaboldi *et al.*: ApJ, **472**, 145 (1996)
14. M. Arnaboldi *et al.*: ApJ, **507**, 759 (1998)
15. A. Romanowsky *et al.*: Science, **301**, 1696 (2003)
16. E. Emsellem *et al.*: MNRAS, **352**, 721 (2004)
17. D. Merritt: ApJ, **413**, 79 (1993)
18. X. Hui *et al.*: ApJ, **449**, 592 (1995); E.W. Peng, H.C. Ford, K.C. Freeman: ApJ, **602**, 685 (2004); M. Arnaboldi *et al.*: ESO Messenger, **76**, 40 (1994)
19. A. Romanowsky: this proceedings
20. A. Toomre: in *The Structure and Evolution of Normal Galaxies*, ed. by B. Tinsley, R. Larson, (Yale Univ. Obs., Newhaven, 1977), p. 401
21. O. Gerhard: MNRAS, **197**, 179 (1981); J. Negroponte, S.D.M. White: MNRAS, **205**, 1009 (1983); J. Barnes: ApJ, **331**, 699 (1988); ApJ, **393**, 484 (1992); L. Hernquist: ApJ, **400**, 460 (1992); J.S. Heyl, L. Hernquist, D.N. Spergel: ApJ, **463**, 69 (1996); T. Naab, A. Burkert: ApJ, **597**, 893 (2004)
22. J. Barnes: Nature, **338**, 132 (1989); M. Weil, L. Hernquist: ApJ, **460**, 101 (1996)
23. J. Barnes, G.P. Efstathiou: ApJ, **393**, 484 (1987); P.J. Quinn, W.H. Zurek: ApJ, **331**, 1 (1988); J.S. Bullock *et al.*: ApJ, **555**, 240 (2001); M. Vivitska *et al.*: ApJ, **581**, 799 (2002)
24. O.E. Gerhard: MNRAS, **265**, 213 (1993)
25. R. Bender: A&A, **229**, 441 (1990); J. Magorrian, D. Ballantyne: MNRAS, **322**, 702 (2001)
26. W. Dehnen, O.E. Gerhard: MNRAS, **261**, 311 (1993)
27. H.-W. Rix *et al.*: ApJ, **488**, 702 (1997); M. Matthias, O.E. Gerhard: MNRAS, **310**, 879 (1999); T.S: Statler, H. Dejonghe, T. Smecker-Hane: ApJ, **117**, 126 (1999); N. Cretton, H.-W. Rix, T. de Zeeuw: ApJ, **536**, 319 (2000); K. Gebhardt *et al.*: AJ, **119**, 1157 (2000); M. Cappellari *et al.*: ApJ, **578**, 787 (2002); K. Gebhardt *et al.*: ApJ, **583**, 92 (2003)
28. R. Bender, R.P. Saglia, O. Gerhard: MNRAS, **269**, 785 (1994)
29. E. Verolme *et al.*: in *Galaxies and Chaos*, ed. by G. Contopoulos, N. Voglis, Lecture Notes in Physics, **626**, 279 (2003)
30. D. Syer, S.D. Tremaine: MNRAS, **282**, 223 (1996); N. Bissantz, V.P. Debattista, O.E. Gerhard: ApJ, **601**, L155 (2004); N. Sambhus, F. de Lorenzi, O.E. Gerhard: this proceedings; F. de Lorenzi, V.P. Debattista, O.E. Gerhard: this proceedings
31. O.E. Gerhard *et al.*: AJ, **121**, 1936 (2001)
32. H.-W. Rix, M. Carollo, K.C. Freeman: ApJ, **513**, L25 (1999)
33. M. Persic, P. Salucci, F. Stel: MNRAS, **281**, 27 (1996)
34. M. Baes, H. Dejonghe: ApJ, **563**, L19 (2001); MNRAS, **335**, 441 (2002)
35. M. Capaccioli *et al.*: ApJ, **371**, 535 (1991); T.S. Statler, T. Smecker-Hane: AJ, **117**, 839 (1999)
36. A. Matthieu, H. Dejonghe, X. Hui: A&A, **309**, 30 (1996)
37. T.H. Puzia *et al.*: A&A, **415**, 123 (2004)
38. T. Richtler *et al.*: AJ, **127**, 2094 (2004)
39. Y. Ikebe *et al.*: Nature, **379**, 427 (1996); M. Paolillo *et al.*: ApJ, **565**, 883 (2002)
40. P. Côté *et al.*: ApJ, **559**, 828 (2001)
41. M. Franx, J.H. van Gorkom, T. de Zeeuw: ApJ, **436**, 642 (1994)
42. F. Bertola *et al.*: ApJ, **416**, L45 (1993); T.A. Oosterloo, R. Morganti, E.M. Sadler: AJ, **123**, 729 (2002)

43. H. Awaki *et al.*: PASJ, **46**, L65 (1994); K. Matsushita *et al.*: ApJ, **499**, L13 (1998); M. Paolillo *et al.*: ApJ, **586**, 850 (2003); D. Buote: ApJ, **577**, 183 (2002)
44. M. Loewenstein, R.E. White: ApJ, **518**, 50 (1999); S. Sato *et al.*: ApJ, **537**, L73 (2000)
45. T.A. McKay *et al.*: ApJ, **571**, L85 (2002); D. Rusin, C.S. Kochanek, C.R. Keeton: ApJ, **595**, 29 (2003)